# Fabrication of microstructures in photoetchable glass ceramics using excimer and femtosecond lasers

**Joohan Kim**
**Halil Berberoglu**
**Xianfan Xu**
Purdue University
School of Mechanical Engineering
West Lafayette, Indiana 47907
E-mail: xxu@ecn.purdue.edu

**Abstract.** We discuss laser fabrication of microstructures in photoetchable glass ceramics called Foturan (Schott Company, Elmsford, NY). A KrF excimer laser ($\lambda = 248$ nm, $\tau = 25$ ns) is used for surface micromachining, and a femtosecond laser ($\lambda = 800$ nm, $\tau = 80$ fs) is used for fabricating 3-D structures. Important aspects of the machining, such as depth of machining resulting from different laser processing parameters and threshold laser fluences, are presented. A detailed analysis of the absorption process of both lasers in photoetchable glass ceramics is provided. 
[DOI: 10.1117/1.1759330]

Subject terms: photoetchable glass ceramics; excimer laser; femtosecond laser; micromachining; 3-D machining.

Paper 03025 received Mar. 5, 2003; revised manuscript received Dec. 19, 2003; accepted for publication Dec. 19, 2003.

## 1 Introduction

Photoetchable glass ceramics are very promising materials for fabricating a variety of microstructures and systems. These materials have high Young's Modulus, transparency in visible wavelengths, and good thermal and electrical insulation properties. In addition, their chemical stability, biocompatibility, and high melting temperatures enable the fabricated microdevices to be used in corrosive and high-temperature environments for a variety of biological and chemical applications.[1] For example, photoetchabe glass ceramics have been used for making high aspect ratio spacers in field emission displays (FED), gas electron multipliers as detectors, and microreactors.[2–4]

To effectively machine microstructures in glass ceramics, it is desirable to find alternative methods that have distinctive advantages compared with conventional lithographic techniques. Laser-based fabrication in photoetchable glass ceramics has been studied for making miniature satellites and other microdevices.[5–7] Photons from the laser beam are used to change material properties locally, followed by a material removal process accomplished by chemical etching. Therefore, the laser-based method combines the advantages of two processes: fast and local patterning using laser beams, and efficient material removal using wet etching. Another advantage is 3-D machining of photoetchable glass ceramics by focusing a laser beam inside the material. This 3-D machining eliminates many difficult assembly steps in microdevice fabrication and packaging. Femtosecond lasers are very useful for making 3-D structures on glass ceramics due to their low absorptivity at the laser wavelength ($\lambda = 800$ nm) except at the focal point where the laser intensity is high enough to cause multiphoton absorption. Embedded 3-D structures such as Y- or H-shaped channels have been produced with femtosecond lasers.[8–11]

A detailed study on laser-based micromachining of photoetchable glass ceramics is presented. The intention is to understand the micromachining process using two different types of lasers, a UV excimer laser and a femtosecond laser. Due to high absorptivity at the excimer laser wavelength ($\lambda = 248$ nm) and the large laser beam size, the excimer laser is mainly used for fabricating complex structures on surfaces. Machining characteristics using different processing parameters are studied. Results obtained from the two lasers are compared. In Sec. 2, the principles of micromachining in photoetchable glass ceramics are reviewed. In Sec. 3, experimental results from this study are presented and analyzed.

## 2 Principles

The photoetchable glass ceramics used for our study, Foturan, are manufactured by Schott Company. The basic idea behind laser processing of photoetchable glass ceramics is to create a way to induce anisotropic chemical etching. Glass is an amorphous material, meaning there are no specific directions within its structure to create directionally specific etching. However, by locally modifying this amorphous structure using irradiation such as a laser beam, it becomes possible to change its etching characteristics and therefore to create designed structures.[5,12] In Foturan, this is achieved by creating a local crystalline phase that etches about 20 times faster than the amorphous one. Processing of Foturan requires three main steps, namely photosensitization, heat treatment, and etching.

### 2.1 *Photosensitization*

Photosensitization is the first step in structuring Foturan, where the structure to be created is written and/or projected onto the material with a suitable light source. During illu-

 1537-1646/2004/$15.00 

mination, local temperature rise induces formation of $Ce^{3+}$ ions. These ions are stabilized by $Sb_2O_3$ and other reducing agents:[13]

$$2Ce^{4+} + Sb^{3+} \leftrightarrow 2Ce^{3+} + Sb^{5+}. \quad (1)$$

The unstable $Ce^{3+}$ ion in turn absorbs enough photon energy from a laser beam, giving away one electron going into the stable $Ce^{4+}$ form.

$$Ce^{3+} + h\nu \rightarrow Ce^{4+} + e^{-}. \quad (2)$$

The created electrons are then absorbed by the silver ions, which are reduced to silver atoms.

$$Ag^{+} + e^{-} \rightarrow Ag. \quad (3)$$

The resulting silver atoms act as nucleation sites, around which lithium metasilicate in Foturan can be crystallized during the heat treatment step. Cheng et al. suggest that silver atoms are created at the heat treatment step, inducing a precise high spatial resolution of the crystallized region, but the exact mechanism is still subject to investigation.[14]

### 2.2 *Heat Treatment*

Following photosensitization, Foturan is heat treated for lithium metasilicate to crystallize around the silver nucleation cites. During this step, it is desirable to obtain as small a crystal size as possible to reduce surface roughness after the etching step. This is quite important for creating microstructures, since uncontrolled crystal sizes ranging from 1 to 10 $\mu$m are possible. Also, it is believed that the crystal sizes can affect the etch ratio between the crystalline phase and the amorphous phase. Although there is no exact recipe for the heat treatment process, several procedures have been proposed in the literature.[15] Accordingly, in our work, Foturan is first heated up to 500 °C at a rate of 5 °C per minute. During this portion of the heat treatment, silver atoms diffuse to form silver clusters in the exposed regions. After staying at this temperature for about an hour, the temperature is ramped up to 605 °C at a rate of 3 °C per second. At this temperature, crystallization is most efficient and the Foturan is held at this temperature for about an hour. Finally, the sample is cooled to room temperature in ambient. Fuqua et al.[15] also mentioned that the formed crystals would have a lower density, so internal stresses and surface roughness would show up to a degree, depending on the size of the structures. Note that the temperature used in this heat-treating process is much higher than the temperature caused in the laser processing step, therefore, crystallization does not occur during laser processing.

### 2.3 *Etching*

The final step in the structuring of Foturan is wet etching. In this step, the crystalline regions are etched away using hydrofluoric acid (HF).

$$Li_2SiO_3 + 8HF \rightarrow 2LiF + H_2SiF_6 + 3H_2O. \quad (4)$$

In the literature, there are several different concentrations and schemes suggested for etching. Dietrich et al. used a solution of 10% HF in an ultrasonic bath or spray etcher at room temperature.[13] Fuqua et al. suggested using 5% HF at 40 °C.[15] Both sources quote an etch ratio of 20 to 1 between the exposed and unexposed region. It is found in our experiments that the aspect ratio and the etch rate are around 10 and 0.5 $\mu$m/min, respectively, which are comparable to the reported values.[16] The etch rate decreases as the dimensions of the structure gets smaller, since HF cannot reach in as effectively. This is one of the biggest problems for creating high aspect ratio and embedded structures, as it can become quite difficult to get the etchant to every part of the structure without broadening the easily accessible sections.

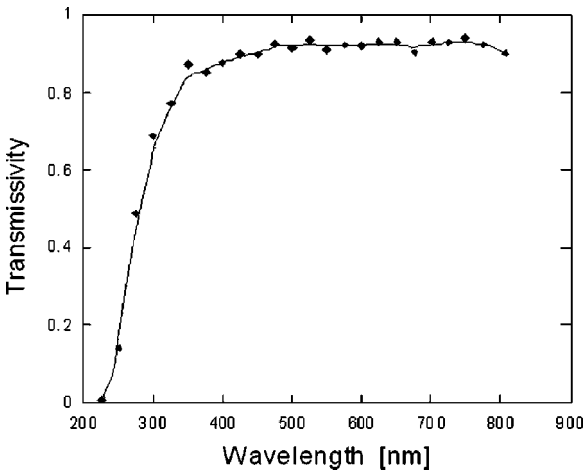


**Fig. 1** Spectral transmissivity of Foturan. The thickness of the sample is 0.2 mm.

## 3 Experiments and Results

The lasers used are a KrF excimer laser (pulsewidth = 25 ns, wavelength = 248 nm) and a Ti:sapphire amplified femtosecond laser (pulsewidth = 80 fs, wavelength = 780 nm). For creating 2-D surface structures using the excimer laser, the image of a mask is projected onto the Foturan surface. In this case, the minimum feature size is limited by the crystallized grain size after the heat treatment, which is around a few microns. In our work, a well-defined pattern can be obtained using a single pulse when the smallest feature size is above 10 $\mu$m. Another method to create a pattern is to scan a beam with a primitive shape, such as a circle along a predetermined path. This latter method is used in both excimer and femtosecond laser processing. Various features can be printed on or inside the material (for the femtosecond laser only) with a proper focusing lens and computer-controlled high precision motion stages. The depths of focus for the excimer laser and the fs laser focusing lenses are 24.3 and 1.6 $\mu$m, respectively.

Figure 1 shows the transmissivity of a 0.2-mm-thick Foturan sample with respect to the wavelength measured using a spectral photometer. At the wavelength of the KrF excimer laser, 248 nm, the transmissivity is 2.6%, indicating that most energy at this wavelength is absorbed in the material in the near surface region. Because of the very low transmissivity at this wavelength, it is rather difficult to focus the laser beam using the focusing lens set into the material for creating embedded structures, and avoid pho-

tosensitizing the surface region. A high numerical aperture objective lens could be used so that only the region under the surface is irradiated with a fluence above the threshold for photosensitization. However, the depth of the photosensitized region using the high numerical aperture objective lens would be shallow, around tens of micrometers, meaning the embedded structure, if it can be made, will not be deeper than tens of micrometers. The femtosecond laser at the wavelength of 780 nm has a high transmissivity (>90%), and the loss is due to surface reflection. When the femtosecond pulses are focused to a tight spot, multiphoton absorption allows effective absorption, causing the reaction shown in Eq. (2). The effective volume where this reaction can take place depends on the depth of focus and the intensity of the focused laser beam. In general, only a small volume of material can be photosensitized by a single pulse, therefore, scanning is needed to create a pattern.

### 3.1 *Excimer Laser for 2-D Machining*

The excimer laser fluences used in this work are in the range from 0.1 to 3.0 J/cm$^2$. A mask with a pattern of a cross in a circle is used for demonstrating projection machining. The laser beam passed through the mask is condensed ten times with a lens set and imaged on the specimen. Different numbers of laser pulses and fluences are applied to evaluate their effects. The irradiated specimens are heat treated and then developed in a 5% HF solution for 1 to 20 min, depending on the crystallized depth of the structure.

The specimen after heat treatment and etching is shown in Fig. 2. The dark areas in Fig. 2(a) are the crystallized region after the heat treatment. More pulses or higher fluence produce a darker region and the depth of crystallization region grows. However, the increase of the depth is not linear.

Figure 3 shows SEM pictures of the etched specimen. The wall surface has many craters where crystallites are formed. Their diameters are on the order of a few microns, which dictate the roughness and the minimum feature size of the structure. The surface of the crystallized region is smoother than that of the noncrystallized region, as shown in Fig. 3(b). It is expected that a smoother surface can be obtained when a higher fluence is used for photosensitization, or other heat treatment parameters are applied, which are shown later in Sec. 3.2.

The depth of the structure after etching is related to the level of crystallization and the etching time. To obtain an expected structure, it is desirable to control the depth of the crystallization region and to etch away the crystallized region only. The crystallization depth with respect to fluence is shown in Fig. 4. One pulse is fired at each fluence. As expected, it is seen that the higher the laser fluence, the deeper the crystallization region. This would allow fabrication of a structure with different depths. The relationship between fluence and crystallization depth follows the simple Beer's law of radiation absorption as:

$$\frac{I}{I_0} = \exp(-\alpha \cdot x), \tag{5}$$

where $I$ is the fluence inside the material at a distance $x$ from the surface, $I_0$ is the incident fluence, and $\alpha$ is the absorption coefficient. Using a curve fit of the measured data, the threshold fluence ($I_{th}$) and absorption coefficient ($\alpha$) are found to be 0.011 J/cm$^2$ and 0.0225 $\mu$m$^{-1}$, respectively.

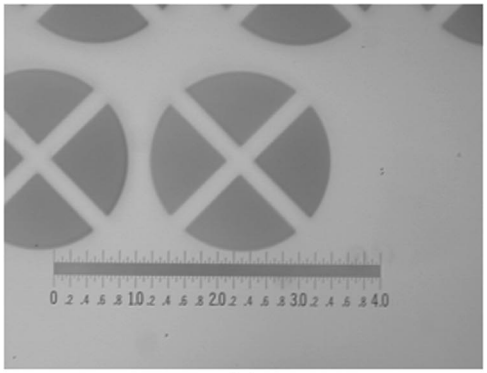


(a)

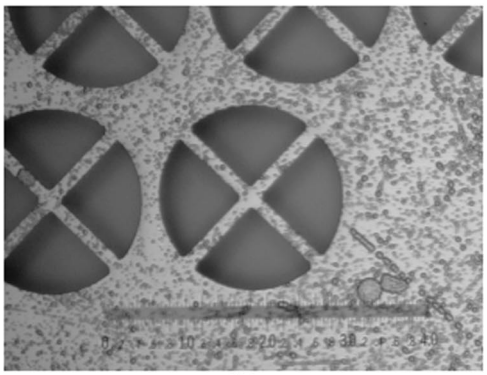

(b)

**Fig. 2** Surface images (a) after heat treatment and (b) after etching process. Full length of the scale is 400 $\mu$m (the diameter of the circle is about 200 $\mu$m) and the excimer laser fluence is 0.1 J/cm$^2$.

The crystallization depth with respect to the number of laser pulses is shown in Fig. 5. The laser fluences are 0.33 and 1.5 J/cm$^2$. An increase of the crystallization depth with respect to the number of pulses is observed. One possibility is that photosensitization by previous pulses changes the absorption coefficient of the material. However, it is found that the absorptivity increases after irradiation. At a laser fluence of about 0.3 J/cm$^2$, the absorptivity increases about 40% after 100 pulses. A more likely explanation is that photosensitization also depends on the total doses (number of photons). This will be confirmed when the results obtained using the femtosecond laser are analyzed. As the number of pulses increases, the crystallization depth levels off. It should be noted that the increase of the depth with the number of pulses is slow. This offers an advantage when the scanning method is used to create a pattern: overlapping of laser pulses that occurs during scanning will not significantly change the depth of photosensitization.

### 3.2 *Femtosecond Laser for 3-D Machining*

Multiphoton absorption is one of the forms of nonlinear absorption where two, three, or more photons are absorbed in a stepwise manner or simultaneously by atoms or molecules. In this way, instead of absorbing a single photon of

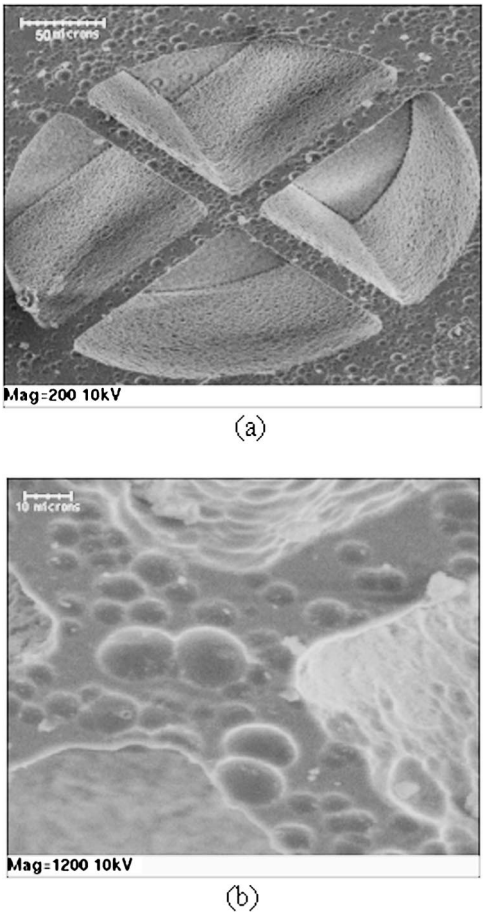


**Fig. 3** SEM images of the etched specimen. The laser fluence is 1.5 J/cm$^2$.

high energy, similar chemical reactions can occur by absorbing a number of photons of lower energy. This is exactly the case in Foturan irradiated by femtosecond laser pulses. Instead of absorbing high-energy UV photons, same chemical reactions can be brought about by absorbing multiple near-IR photons.

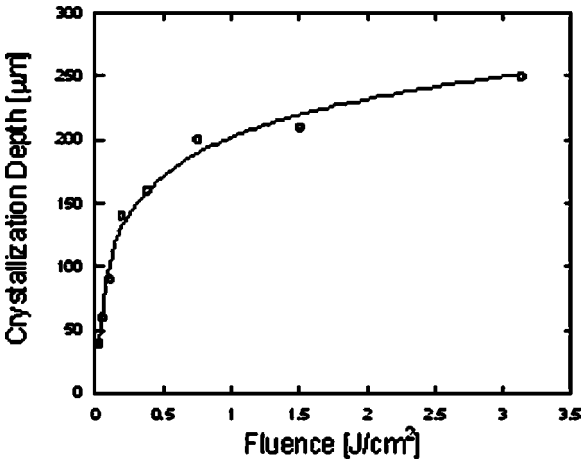


**Fig. 4** Crystallization depth as a function of laser fluence (single pulse).

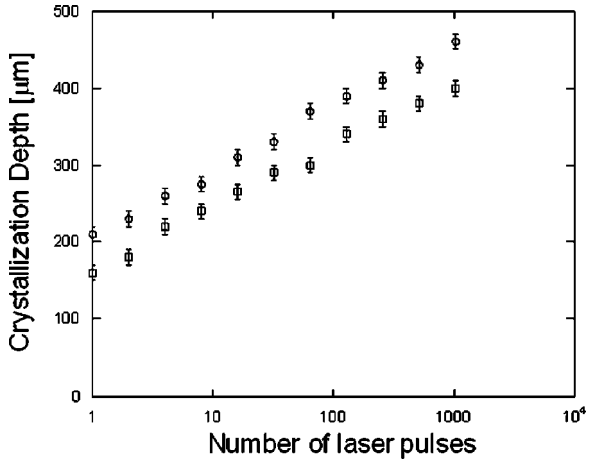


**Fig. 5** Crystallization depth as a function of the number of laser pulses. (□: 0.33 J/cm$^2$ and ○: 1.5 J/cm$^2$.)

To investigate the multiphoton absorption process, a simple experiment was designed to determine how many photons are actually involved in the process. In this experiment, it is assumed that absorption is related to the incident intensity $I$ as:

$$\frac{dI}{dx} = -\alpha I^n, \tag{6}$$

where $I$ is the incident intensity in W/cm$^2$, $\alpha$ is the nonlinear absorption coefficient, $n$ is the number of photons absorbed, and $x$ is the distance from the surface to which the laser is incident on, measured in centimeters. Integrating this expression over the sample length $L$ gives Eq. (7), which can be utilized together with the data to determine $n$ and $\alpha$.

$$I^{(1-n)} - I_o^{(1-n)} = (n-1)\alpha L. \tag{7}$$

The schematic of the experimental setup is shown in Fig. 6. In this setup, the sample is slightly tilted so that the reflected portion of the intensity could be detected easily. The detector used in the experiment is a power meter. The same detector is used at three different locations, namely Det 1, Det 2, and Det 3, to measure the input power, the transmitted power, and the reflected power, respectively. The lens used has a 200-mm focal length, which gives a spot size of 78 $\mu$m diam. Using this lens, the Rayleigh length is about 6.3 mm, which provides a weak focusing

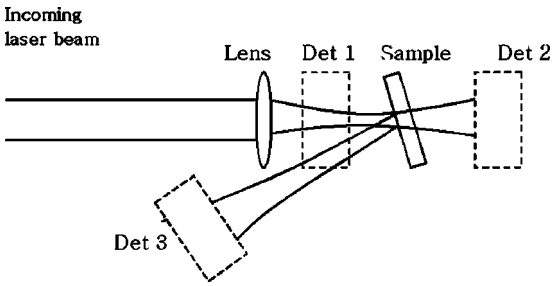


**Fig. 6** Schematic of the multiphoton absorption experiment.

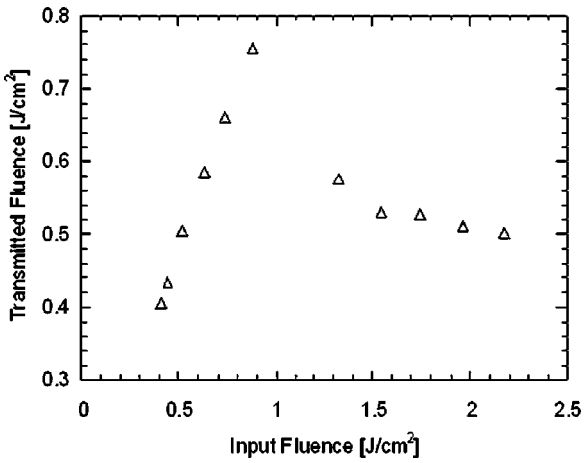


**Fig. 7** Transmitted fluence versus input fluence.

condition for the 0.3 mm Foturan sample. In this experiment, transmission measurements up to surface ablation, which took place for input fluences greater than 4 J/cm$^2$, were conducted. The obtained transmitted power versus input power is shown in Fig. 7. From this figure, it can be seen that there is a regime change at about 1 J/cm$^2$. This regime change is due to the optical damage, distinct from the ablative damage occurring. A similar trend change can also be observed in Fig. 8, which shows the plot of transmissivity versus the input fluence.

From Fig. 8, it can be seen that the first three data points correspond to a transmittance of about 1, which indicates that there is no absorption. (Contribution of surface reflectivity has been deducted from the results.) Therefore, the data for input fluence between 0.6 and 1 J/cm$^2$ were utilized in investigating the multiphoton absorption process. A code was written to perform a nonlinear fit to the data and to estimate the value of $n$ and $\alpha$. This method estimated the value of $n$ to be 3.09 and the value of $\alpha$ to be 6.22 $\times 10^{-7}$ cm$^3$ W$^{-2}$. This result clearly signifies that the multiphoton absorption process in Foturan is a three photon process, which is reasonable, since the combined energy of three photons is 4.6 eV ($\lambda = 260$ nm), which is well into

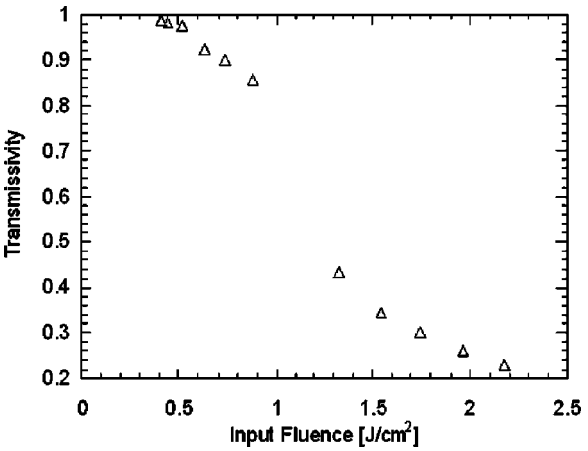


**Fig. 8** Transmissivity versus input fluence.

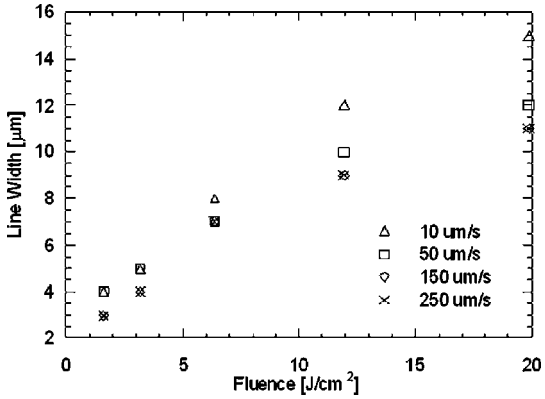


**Fig. 9** Line width as a function of laser fluence and write speed.

the absorption region according to Fig. 1. On the other hand, the energy of two photons is not high enough to be absorbed.

Characterization experiments are needed to understand how the crystallization depth and width change with laser intensity and scanning speeds, and how different heat treatment conditions affect the crystal structure. The first experiment was designed to obtain the cross sectional width and depth of the crystallized region with respect to laser power and write speed. During this experiment, a Mitutoyo M Plan Apo $-20\times$ microscope objective lens (Kawaski, Kanagawa, Japan) is utilized, which gives a theoretical diameter of 4 $\mu$m. The laser fluences are calculated from this theoretical value. However, it is believed that the actual diameter of the laser spot on the sample could be a few times larger due to the rather poor beam quality. Therefore, the laser fluences indicated next are used only for finding relative fluences and the trend of machining results. After photosensitization, the sample is heat treated with the procedure described earlier. Then, the sample is visually inspected to determine the crystallized region and the respective dimensions. Lines with five different fluence levels and four different speeds are obtained and analyzed.

The results of the experiment are presented in Figs. 9 and 10. Some error could have been introduced in the line

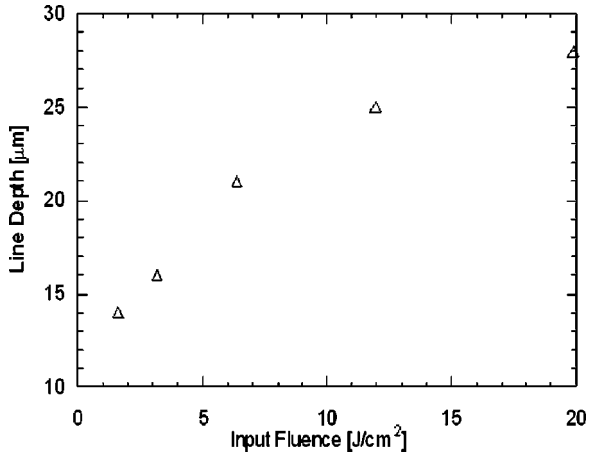


**Fig. 10** Line width as a function of fluence when the speed is fixed at 50 $\mu$m/s.

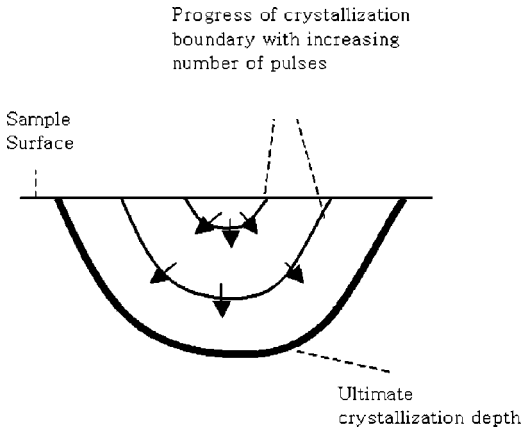


**Fig. 11** Progression of line thickness and depth.

width measurements at lower fluence levels and high write speeds, for which the resolution of the measuring technique was not sufficient to determine the occurring changes exactly. From these figures, it is seen that the line width is dependent on fluence. However, for different speeds at a fixed fluence, this relation changes in a power form. These results suggest that for a given laser fluence, the line thickness increases to an ultimate value with an increasing number of pulses. In Fig. 11, the progression of the crystallization depth with increasing number of pulses is illustrated. As discussed before, the femtosecond pulses are absorbed via multiphoton absorption. As the number of pulses increases, more regions receive enough photons to cause nucleation. Hence, the volume where nucleation can take place increases. The crystallization volume eventually levels off, where the energy density of pulses decreases to a level at which nonlinear absorption can no longer take place.

The second experiment investigated the etch depth as a function of laser fluence and write speed. Results of the experiment are presented in Fig. 12. During the experiment, the samples are etched for 20 min and the profiles are measured using a profilometer. From these results, it can be seen that the etch depth decreases with decreasing fluence and increasing write speed. The trend for the write speed

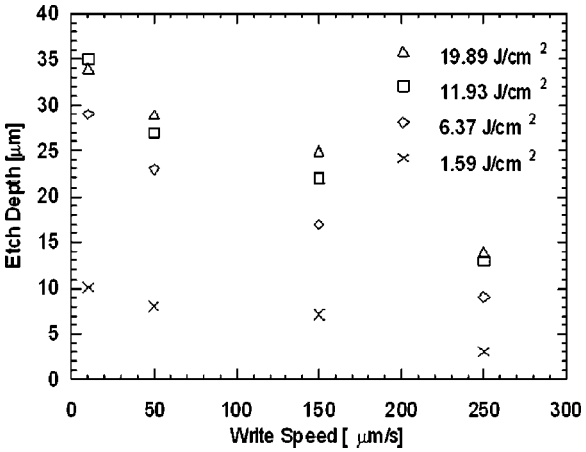


**Fig. 12** Etch depth comparison for different fluences and write speeds.

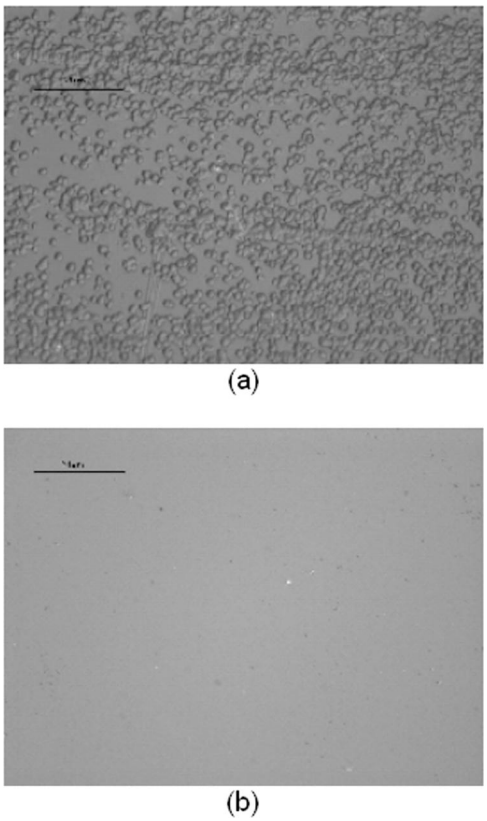


**Fig. 13** Nomarski pictures of surface quality (a) before and (b) after second baking taken with 40× objective. The length of the scale bar is 24 μm.

suggests that the longer a particular area is irradiated, i.e., more pulses per area, the deeper it etches. This is the same as observed in the excimer laser experiment, where the etch depth also increases with the number of laser pulses due to the accumulation of the photons received at a certain depth. Also similar to the excimer laser experiment, a higher intensity causes deeper etching. Therefore, using high fluence would allow higher aspect ratio features to be created.

The surface quality after etching can be seen in Fig. 13(a). Same as excimer laser processing, surface roughness is developed after etching. To obtain smoother etch surfaces, a second heat treatment was tested. The idea was to melt the surface slightly without warping the structure. The samples were heated in an oven to 650 °C for half an hour and cooled to room temperature. Images of samples after the second heating process are shown in Fig. 13(b). It can be seen that the surface roughness is much reduced. It is not known if optical or mechanical properties are affected by the second heat treating, since no visible changes can be identified except the decrease of surface roughness. This procedure can also be applied to the excimer laser processed sample to reduce roughness. It should be noted that heating the sample to 650 °C in the first heat treatment does not reduce the roughness, because the roughness is developed during the etching process.

3-D microstructuring using femtosecond pulses is demonstrated by creating a U-shaped channel in Foturan. After obtaining some basic parameters involved in femtosecond laser structuring of Foturan, a U-shaped channel was de-

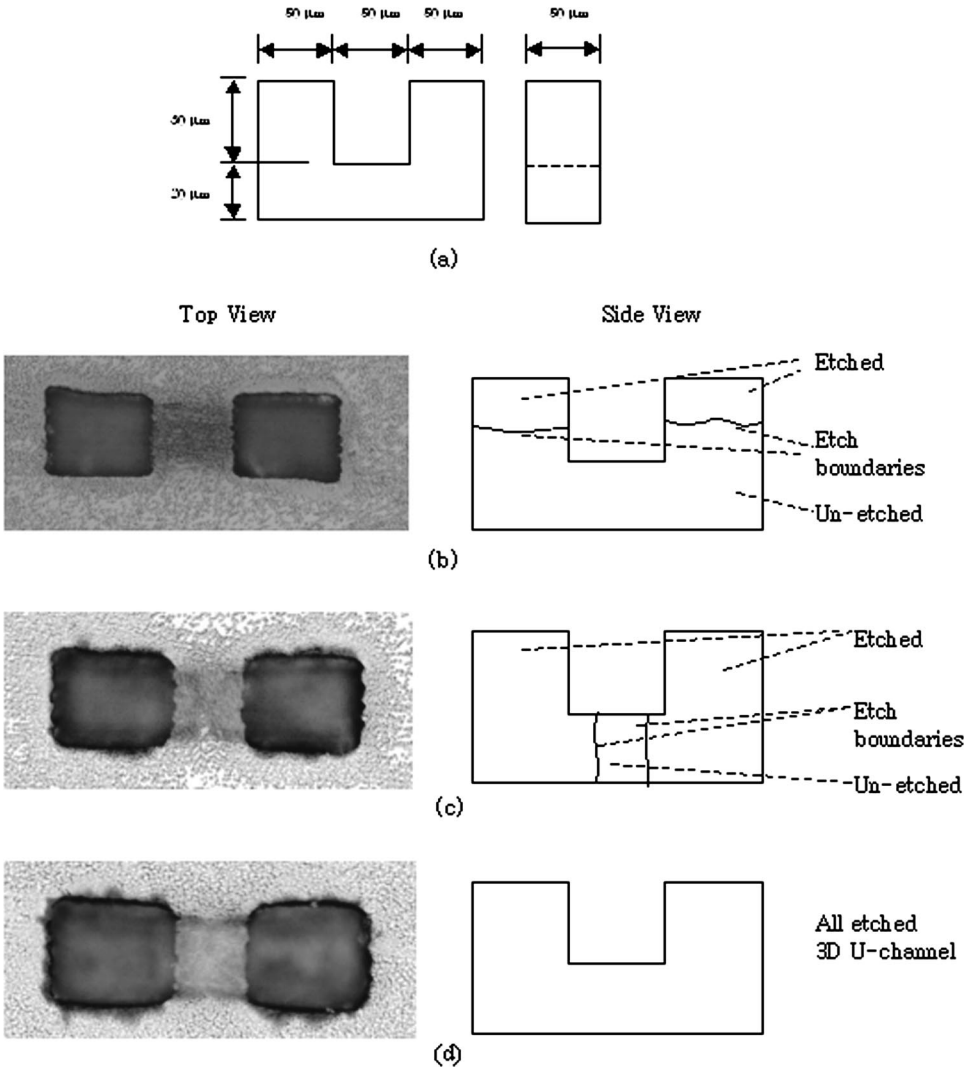


**Fig. 14** (a) Design of the U-shaped channel. (b), (c), and (d) Left: Nomarski pictures (top view) of the etch progress of the U-shaped channel. The illustrations at right are side views showing the progress of the etching.

signed to demonstrate 3-D machining. The dimensions of the design are given in Fig. 14(a). The channel was written in Foturan with 3.18 J/cm$^2$ at a speed of 50 $\mu$m/sec. These correspond to a line width of 5 $\mu$m and a line depth of 16.5 $\mu$m. Layer-by-layer scanning is performed from the bottom to the top layer by adjusting the laser focusing depth. The etching is performed in 5% hydrofluoric acid (HF) solution for about 45 min. The progress of etching is observed as presented in Figs. 14(b), 14(c), and 14(d). In Fig. 14(b), the arms of the U-shaped channel are etched and the etching of the connecting bottom layer has not started yet. In Fig. 14(c), the etching of the connecting layer is progressing. In Fig. 14(d), the etching of the bottom connecting layer has been completed, creating a 3-D U-shaped channel in Foturan.

## 4 Conclusions

We investigate laser processing of photoetchable glass ceramic, Foturan, using a UV excimer laser and a near-IR femtosecond laser. The different wavelengths of the lasers demonstrate different processing characteristics. The excimer laser irradiation at a wavelength of 248 nm has a very low transmissivity in Foturan; hence, it is useful for fabricating structures on the surface. The spatially uniform, large excimer laser beam allows machining of a large pattern using only one laser pulse. On the other hand, very high transmissivity and multiphoton absorption of femtosecond laser irradiation at a wavelength of 800 nm make it possible to produce a 3-D structure by focusing and scanning the laser pulses inside the specimen. Along the way, parameters required for processing Foturan with excimer and femtosecond laser pulses are studied. The threshold fluence and relations between fluence and crystallization dimensions are obtained. Interaction between the 800-nm fs pulse and Foturan is determined to be a three-photon absorption process.

### *Acknowledgments*

This work is supported by the Integrated Detection of Hazardous Materials (IDHM) Program, a Department of Defense project managed jointly by the Center for Sensing Science and Technology, Purdue University and the Naval

Surface Warfare Center, Crane, Indiana, and the Office of Naval Research. The authors also thank Sreemanth Uppuluri and Ihtesham H. Chowdhury for help on the experiments.

## References


1. J. W. Schultze and V. Tsakova, ''Electrochemical microsystem technologies: from fundamental research to technical systems,'' *Electrochim. Acta* **44**, 3605–3627 (1999).
2. Y. R. Cho, J. Y. Oh, H. S. Kim and H. S. Jens, ''Micro-etching technology of high aspect ratio frameworks for electronic devices,'' *Mater. Sci. Eng.* **B64**(2), 79–83 (1999).
3. S. K. Ahn, J. G. Kim, V. Perez-Mendez, S. Chang, K. H. Jackson, J. A. Kadyk, W. A. Wenzel, and G. Cho, ''GEM-type detectors using LIGA and etchable glass technologies,'' *IEEE Trans. Nucl. Sci.* **49**(3), 870–874 (2002).
4. K. Yunus, C. B. Marks, A. C. Fisher, D. W. E. Allsopp, T. J. Ryan, R. A. W. Dryfe, S. S. Hill, E. P. L. Roberts, and C. M. Brennan, ''Hydrodynamic voltammetry in microreactors: multiphase flow,'' *Electrochem. Commun.* **4**, 579–583 (2002).
5. P. Fuqua, S. W. Janson, W. W. Hansen, and H. Helvajian, ''Fabrication of true 3D microstructures in glass/ceramic materials by pulsed UV laser volumetric exposure techniques,'' *Proc. SPIE* **3618**, 213–220 (1999).
6. W. Hansen, P. Fuqua, F. Livingston, A. Huang, M. Abraham, D. Taylor, S. Janson, and H. Helvajian, ''Laser fabrication of glass microstructures,'' *Industrial Physicist*, pp. 18–21 (June/Jul. 2002).
7. A. Huang, W. W. Hansen, S. W. Janson, and H. Helvajian, ''Development of a 100 gm class inspector satellite using photostructurable glass/ceramic materials,'' *Proc. SPIE* **4637**, 297–304 (2002).
8. Y. Kondo, J. Qiu, T. Mitsuyu, K. Hirao, and T. Yoko, ''Three-dimensional microdrilling of glass by multiphoton process and chemical etching,'' *Jpn. J. Appl. Phys., Part 2* **38**(10A), L1146–L1148 (1999).
9. A. Marcinkevicius and S. Juodkazis, ''Femtosecond laser-assisted three-dimensional microfabrication in silica,'' *Opt. Lett.* **26**(5), 277–279 (2001).
10. Y. Cheng, K. Sugioka, K. Midorikawa, M. Masuda, K. Toyoda, M. Kawachi, and K. Shihoyama, ''Control of the cross-sectional shape of a hollow microchannel embedded in photostructurable glass by use of a femtosecond laser,'' *Opt. Lett.* **28**(1), 55–57 (2003).
11. M. Masuda, K. Sugioka, Y. Cheng, N. Aoki, M. Kawachi, K. Shihoyama, K. Toyoda, H. Helvajian, and K. Midorikawa, ''3-D microstructuring inside photosensitive glass by femtosecond laser excitation,'' *Appl. Phys. A: Solids Surf.* **76**, 857–860 (2003).
12. I. Rajta, I. Gomez-Morilla, M. H. Abraham, and A. Z. Kiss, ''Proton beam micromachining on PMMA, Foturan and CR-39 materials,'' *Nucl. Instrum. Methods Phys. Res. B* **210**, 260–265 (2003).
13. T. R. Dietrich, W. Ehrfeld, M. Lacher, M. Kramer, and B. Speit, ''Fabrication technologies for microsystems utilizing photoetchable glass,'' *Microelectron. Eng.* **30**, 497–504 (1996).
14. Y. Cheng, K. Sugioka, M. Masuda, K. Shihoyama, K. Toyoda, and K. Midorikawa, ''Optical gratings embedded in photosensitive glass by photochemical reaction using a femtosecond laser,'' *Opt. Express* **11**(15), 1809–1816 (2003).
15. P. D. Fuqua, D. P. Taylor, H. Helvajian, W. W. Hansen, and M. H. Abraham, ''A UV direct-write approach for formation of embedded structures in photostructurable glass-ceramics,'' *Mater. Res. Soc. Symp. Proc.* **624**, 79–86 (2000).
16. F. E. Livingston, W. W. Hansen, A. Huang, and H. Helvajian, ''Effect of laser parameters on the exposure and selective etch rate in photostructurable glass,'' *Proc. SPIE* **4637**, 404–412 (2002).


**Joohan Kim** received his BEng (1996) and MSc (1997) degrees in mechanical engineering from Ajou University and University of Manchester Institute of Science and Technology (UMIST), respectively. He is currently working toward his PhD degree at the Center for Laser Microfabrication at Purdue University. His main interests lie in laser fabrication of polymer microfluidic devices and polymer replication techniques.

**Halil Berberoglu** received his BS (2000) and MS (2003) degrees in mechanical engineering from Purdue University. He is currently a PhD student at the University of California, Los Angeles.

**Xianfan Xu** is an associate professor at the School of Mechanical Engineering and the director of the Center for Laser Microfabrication of Purdue University. He received his MS and PhD degrees in mechanical engineering in 1991 and 1994 respectively, both from the University of California at Berkeley. His current research interests include laser micro- and nanofabrication, and fundamental studies of laser material interactions.